Ceramics International 49 (2023) 18565–18576

Contents lists available at ScienceDirect

Ceramics International

journal homepage: www.elsevier.com/locate/ceramint

Biomimetic mineralized amorphous carbonated calcium phosphate-polycaprolactone bioadhesive composites as potential coatings on implant materials

Monika Furko [a,*], Rainer Detsch [b], István Tolnai [a], Katalin Balázsi [a], Aldo R. Boccaccini [b,**], Csaba Balázsi [a]

[a] Centre for Energy Research, ELKH, H-1121 Konkoly-Thege rd. 29-33, Budapest, Hungary
[b] University of Erlangen-Nuremberg, Department of Materials Science and Engineering, Institute of Biomaterials, Cauer str. 6, 91058, Erlangen, Germany

ARTICLE INFO

Keywords:
Bioceramics
Amorphous calcium phosphate
Biopolymers
Composites
Biodegradability

ABSTRACT

Biomimetic mineralized (Mg, Zn, Sr) carbonated amorphous calcium phosphate (cACP) containing biodegradable polycaprolactone (PCL) coating was prepared via spin coating technology. The main role of PCL was to provide a controlled release of cACP for a prolonged period of time and to act as a bioadhesive, providing better adherence than that of pure cACP powder. The cACP and the cACP-PCL composite layers were optimized as very thin, non-continuous films on the surface of a commercial titanium alloy, maintaining its surface roughness. The powder layer and the composite film were morphologically, chemically, and biologically tested. *In vitro* biocompatibility measurements were performed using MC3T3-E1 cells. The cell viability significantly increased when cACP coatings and cACP-PCL composite were applied to the pure Ti6Al4V substrate. The pure PCL coating and the titanium substrate indicated similar biocompatibility, however, adding cACP powders into the polymer solution resulted in increased cell viability. LDH and ALP measurements showed a large number of living cells on the surface of all samples. The cell morphology study by Calcein/DAPI staining as well as SEM measurements demonstrated a well-adhered and spread, confluent cell monolayer. The long-term release of bioactive ions in SBF solution indicated that the biodegradability of composite coating is slightly faster than the cACP powder layer. All *in vitro* measurements confirmed the suitability of the developed composite layer as a potential bone substitute and bioactive coating on middle- and long-term implants.

1. Introduction

The surfaces of load-bearing orthopedic metallic implants can be modified by depositing ceramic particles or polymer layers as well as ceramic/polymer composites [1]. Owing to this modification, the process of osseointegration can accelerate and the possibility of early implant failure can decrease [2–4]. Calcium phosphate (CaP) coatings for metallic implant materials are still a widely researched field. The CaPs are well tolerated by the human body and can induce new bone ingrowth while increasing fixation stability [5,6]. Many *in vivo* results revealed a more rapid connection between bone and implant devices (both orthopedic and dental) in the presence of CaPs [7,8]. The CaP coatings on the surface of the implants support osteoinduction by increasing the levels of calcium and phosphorus ions in the surrounding tissues, which leads to the induction of natural apatite (Ap) on the surface of the implant [8–11]. Amorphous calcium phosphate (ACP) is a precursor phase of HAp and plays a great part in the mineralization processes. ACP has good bioactivity and a controllable biodegradation rate. ACP coatings have also been reported to increase alkaline phosphatase activity, promote cell adhesion as well as improve cell proliferation and growth [12]. Clinical trials on ACP revealed that it can easily transform into bone apatite *in vivo* (through water-induced re-crystallization processes), thus making it an excellent material as either bone defect replacement material or bioactive coating [11,13,14]. Moreover, owing to its amorphous structure, the ACP's solubility is higher than that of more crystalline HAp, therefore, its biodegradation process will be faster [15–17]. *In vivo* studies have also proven that ACP favors a fast fixation of the prosthesis to bone tissue and, additionally, can entrap

* Corresponding author.
** Corresponding author.
E-mail addresses: furko.monika@ek-cer.hu (M. Furko), aldo.boccaccini@fau.de (A.R. Boccaccini).

https://doi.org/10.1016/j.ceramint.2023.02.231
Received 7 December 2022; Received in revised form 13 February 2023; Accepted 27 February 2023
Available online 28 February 2023

higher amounts of bioactive molecules compared to crystalline CaPs [18,19]. In bone minerals, the calcium-to-phosphate molar ratio varies in the range of 1.37–1.87 compared with that of 1.67 for stoichiometric HAp [20]. In addition, carbonate is found to be the most common anionic substituent with a 3–8 wt.% concentration in bone minerals. Carbonate groups can incorporate into the apatitic structure by replacing phosphate and/or hydroxyl groups to form carbonated calcium phosphate phases (cACPs) [21].

On the other hand, biodegradable polymers have also attracted considerable attention as biomaterials in pharmaceutical, medical, and biomedical engineering applications. PCL is an aliphatic polyester that has the favorable features of biodegradability and biocompatibility. The advantage of these polyesters is their biocompatibility and higher hydrolysability in the human body. PCL can be used in many biomedical areas, such as controlled-release drug delivery systems [22], absorbable surgical sutures [23], three-dimensional (3D) scaffolds [24], and biodegradable coatings [25]. The PCL's degradation process is based on the hydrolysis of its ester linkages in physiological conditions. PCL is a very promising material for the preparation of middle- and long-term implantable devices since its degradation are slower than that of polylactide [26,27]. It was also noted that the homopolymer PCL has a total degradation of two to four years (depending on the starting molecular weight of the device or implant) [28,29].

In the scientific literature, the preparation and complex morphological, chemical, and biological characterization of bioresorbable, thin cACP-PCL coatings have been rarely reported so far. In our work, we have combined the advantages of both cACP and PCL in order to achieve a better adhered, more biocompatible very thin bioactive layer onto metallic implant surfaces. In addition, *in vitro* testing was performed to reveal the biocompatible characteristics of the developed novel coatings.

2. Materials and methods

2.1. Materials

Ti6Al4V alloy disks (diameter: 10 mm; thickness: 2 mm) were purchased from Protetim Kft, Hungary. The surface of all titanium discs was roughed by sandblasting, according to the protocol for commercially available implant materials (ISO 5832–2:2018). Calcium gluconate ($HOH_2C(CH(OH))_4COOCa$, Acros Organics, 99%), magnesium gluconate ($HOH_2C(CH(OH))_4COOMg$, VWR International Ltd., ≥98%, high purity), zinc gluconate anhydrous ($HOH_2C(CH(OH))_4COOZn$, VWR International Ltd. - ≥99.0%, AnalaR NORMAPUR) and strontium chloride ($SrCl_2{\cdot}6H_2O$, VWR International Ltd. - ≥99.0%, AnalaR NORMAPUR) then 1 M disodium hydrogen phosphate (Na_2HPO_4, VWR International Ltd. - 99%, AnalaR NORMAPUR), Na_2CO_3 anhydrous, (VWR International Ltd. - ≥99.5% ACS, PCL (polycaprolactone, average M_w ~80,000, Sigma-Aldrich), Dichlorometane (DCM, ACS reagent, ≥99.5%, Merck KGaA, Darmstadt, Germany), Cell viability measurements with WST-8 reagent: Cell counting Kit 8 (Sigma Aldrich), LDH-activity quantification kit (TOX7, Sigma-Aldrich), ALP-Mix (pH = 9.8) (0,1 M Tris, 2 mM $MgCl_2$, (Merck, Germany). and 9 mM p- Nitro Phenyl Phosphate p-NPP (Merck, Germany), p- Nitro Phenyl Phosphate p-NPP (Merck, Germany), calcein acetoxymethyl ester (Calcein AM, Life Technologies, Darmstadt, Germany), DAPI (4,6-diamidino-2-phenylindol, Life Technologies, Darmstadt, Germany).

2.2. Synthesis of bioactive ion-doped biomimetic amorphous carbonated calcium phosphate powder

Suspensions for wet precipitation of bioactive ion-doped cACP were prepared by dissolving calcium gluconate, magnesium gluconate, zinc gluconate anhydrous, and strontium chloride in calculated concentrations in which the Ca:Mg:Zn:Sr ratio was set as 97:2.5:0.45:0.05 in weight percent which is the reported elemental composition of human bone [30,31]. Then 1 M disodium hydrogen phosphate (Ca:P mole ratio adjusted to 5:3) was added into the solution dropwise under vigorous stirring with a magnetic stirrer (1400 rpm) at room temperature. White precipitation was formed right after the addition of phosphorus precursor into the solution. The pH value of the suspensions was adjusted to 11 by adding dropwise an appropriate amount of sodium carbonate anhydrous in order to obtain carbonated ACP particles. The formed suspension was further stirred for 4 h at 80 °C and at 1400 rpm and then left to settle and cool to room temperature. Finally, the white precipitate was washed 3 times using distilled water and dried at 150 °C in an oven for 4 h. The powder was collected and used for further characterization and for the spin coating process.

2.3. Preparation of cACP/PCL composite coatings by spin coating

Polycaprolactone (PCL) was used as a biopolymer and bioadhesive. The pure PCL layer was deposited onto the metallic surface by spin coating technique (Chemat Technology Spin Coater KW-4A, Chemat Scientific Inc, CA, USA). The concentration of the polymer solution was 10% (w/v) in dichloromethane (DCM) solvent. In order to form PCL polymer thin layers loaded with cACP particles, first the cACP particles were dispersed in DCM in 5% (w/v) concentration, then the polymer solution (10% (w/v)) and the cACP (5% (w/v)) suspension was mixed thoroughly in 2:1 wt ratio. The mixture was dropped onto the implant's surface in 200μl/surface area and the spin coating was performed in two steps. First, 300 rpm was applied for homogeneous distribution of suspension, and second, 1000 rpm for solvent evaporation at room temperature. For the preparation of pure PCL coating, only the 10% (w/v) polymer solution was used in spin coating, while in the case of cACP powder coating, only the 5% (w/v) suspension in DCM was used.

2.4. Characterization methods

2.4.1. Morphological characterizations

The morphological studies of cACP powder, the pure PCL layer and cACP-PCL composite layer as well as the MC3T3-E1 pre-osteoblast cell-seeded samples were carried out by field emission scanning electron microscope (SEM, Thermo Scientific, Scios2, Waltham, MA, US) and Energy Dispersive X-ray Spectrometry (Oxford Instrument EDS detector X-Max^n, Abingdon, UK). Map sum spectrum was recorded on samples using 6 keV accelerating voltage. FIB measurements were done with LEO 1540XB Crossbeam workstation. The ion beam parameters in FIB milling mode were 30 kV accelerating voltage and 5 nA beam current. For SEM/FIB measurements the samples were tilted at 52°.

2.4.2. Microstructure study

The surface microtopography and roughness of the samples were further evaluated by an optical microscope (Keyence VHX-6000, KEYENCE Corporation, Osaka, Japan).

2.5. In vitro biocompatibility tests

2.5.1. Cell culture

All the samples were cleaned and sterilized at 130 °C in an autoclave (Systec, Germany) before cell culture. An osteoblast-like cell line, derived from mouse calvaria and denoted MC3T3-E1 (DSMZ, Germany) was used. The cells were cultured at 37 °C in a humidified atmosphere of 95% air and 5% CO_2, in alpha-modified essential medium (α-MEM, Gibco, Germany) containing 10% (v/v) fetal bovine serum (FBS, Sigma-Aldrich, Germany) and 1% (v/v) penicillin/streptomycin (Sigma-Aldrich, Germany). Cells were grown to confluence in 75 cm2 culture flasks (Nunc, Denmark), harvested using Trypsin/EDTA (Sigma, Germany), counted by a coulter counter (Beckman, Germany), and diluted to a concentration of 100000 cells/mL cell culture medium. The sterilized samples were placed into a 24-well plate (Greiner, Germany). Afterward, 1 mL cell suspension was pipetted onto the surface of the

samples as well as on the plastic of the well plate, which was used as a positive control. The proliferation of the MC3T3-E1 cells was analyzed by means of cell counting. The adherent cells were first detached from the surface by Trypsin/EDTA and then counted by coulter counter.

2.5.2. Cell viability

The viability of the pre-osteoblast cells was assessed by applying a WST-8 assay (Sigma-Aldrich) after cultivation periods of 1, 3, 7, and 14 days. Culture media was removed every third day from the 24-well culture plate and the cells were washed with PBS. After the addition of 200 μl of the solution containing 1% (v/v) WST-8 in each well, the plates were incubated for 1.5 h. Subsequently, the supernatant of all samples was transferred to a 96-well plate and the absorbance was measured with an Elisa plate reader (PHOmo, anthos Mikrosysteme GmbH, Germany) at 450 nm. In this colorimetric assay, the UV/VIS absorbance at 450 nm is directly proportional to the amount of dehydrogenase activity in the cell grown on the sample.

2.5.3. Cell amount

Lactate dehydrogenase (LDH) activity provides a measurement of the number of attached cells on the samples. A commercially available LDH-activity quantification kit was used to quantify cell number by the LDH enzyme activity in cell lysate. The MC3T3-E1 cells were cultured in 24-well plates for 7 and 14 days, then washed with PBS and lysed with lysis buffer for 30 min (1 mL/well). Lysates were centrifuged for 5min. at 2000 rpm and 140 μl from the supernatant solutions were pipetted into a 96-well plate. Then, 60 μl LDH-Mix (containing 20 μl of LDH Assay Substrate Solution, 20 μl of LDH Assay Dye Solution, and 20 μl of LDH Assay Cofactor Solution) was added to each sample. The plates were left for 30 min in the dark and the reaction was stopped with 300 μl 1 N HCl per well. The dye concentration was measured with an Elisa plate reader at 490 nm and 690 nm.

2.5.4. Alkaline phosphatase enzyme activity

The alkaline phosphatase (ALP) is one of the first osteoblastic markers. This specific enzyme activity was measured after 7 and 14 days of incubation, in order to characterize the osteoblastic activity of the pre-osteoblast cells. According to the measurement protocol, first, the supernatant from the samples was removed and they were washed with PBS three times. Then, 1 mL 1:9 diluted lysis buffer was added to the samples and incubated for 30min. After incubation, the lysate was removed from the samples and centrifuged for 5 min at 2000 rpm. 100 μl of the supernatant was pipetted into a 96-well plate and 100 μl of ALP-Mix (pH = 9.8) and 9 mM p-NPP were added into each well, mixed, and incubated in the dark for 100 min until the yellowish color change appeared. The reaction was stopped with 650 μl 1 M NaOH and the yellow solution was spectrometrically read at 405 nm and 690 nm with an Elisa plate reader. During the incubation, the p-NPP was transformed into p-NP (para-Nitrophenol) and inorganic phosphate in the presence of an ALP molecule.

2.5.5. Cell distribution

2.5.5.1. Calcein staining. Live staining of the cells was performed using calcein acetoxymethyl ester after 1 day of cultivation. Fluorescence microscopy (FM) (Axio Scope A.1, Carl Zeiss Microimaging GmbH) was used to take images of calcein-stained cells. After the cultivation period of 48 h, the adherent cells were fixed with 3.7% (v/v) paraformaldehyde for 10 min and permeabilized with 0.1% (v/v) Triton X-100 (in PBS) for 10 min at room temperature.

2.5.5.2. DAPI (4,6-diamidino-2-phenylindol) staining. The nuclei of fixed cells were stained with the fluorescence dye 4,6-diamidino-2-phenyl indol (DAPI, Sigma–Aldrich, USA). For staining of the samples, the matrices were incubated for 15 min in the dark in DAPI-solution (2 mL DAPI-stock solution in 1 mL DAPI buffer). The nuclei were imaged by the fluorescence microscope with a blue filter.

2.5.6. Cell morphology

For SEM analysis, the cell cultures were washed with PBS, and fixed with a solution containing 3% (v/v) glutaraldehyde (Sigma, Germany) and 3% (v/v) paraformaldehyde (Sigma, Germany) in 0.2 M sodium cacodylate buffer (pH 7.4), and finally rinsed three times with PBS. All samples were dehydrated in a graded ethanol series (30, 50, 75, 90, 95, and 99.8% (v/v)). Samples were maintained at 99.8% (v/v) ethanol and critical-point dried. No further surface treatment was used prior to the SEM examination.

2.5.7. Statistical analysis

The differences between experimental groups were evaluated by one-way analysis of variance (ANOVA, Origin 2021, OriginLab Corporations, USA). For the comparison of the mean values, the Tukey test was used. The level of statistical significance was given by a *P*-value of 0.05. A *P* value lower than 0.05 was considered statistically significant. *P*-values were more highly statistically significant when $^{**}p < 0.01$, $^{***}p < 0.001$. The number of samples per group was N = 3 or 6.

2.6. Degradation of cACP coating and cACP_PCL composite coating

To determine the exact elemental ratio in cACP powder and to follow the dissolution of different ions of the coatings, an inductively coupled plasma–atomic emission spectroscopy (ICP-AES) technique with ICP-AES spectrometer (Spectro, Spectro Arcos) was used. The measurement was performed in a cyclone fog chamber in the presence of an internal standard (1 ppm Y). Four-point calibration was applied, and standard solutions in concentrations of 0.01, 0.1, 1, and 10 ppm were recorded for each element. The cACP powder was dissolved in 5 mL 1 N HCl solution to determine the elemental composition. For following the long-term dissolution rate of cACP powder and cACP-PCL coating, the samples were immersed in 5 mL SBF solution (conc. in mM: Na^+: 142, K^+: 5, Mg^{2+}: 1.5, Ca^{2+}: 2.5, Cl^-: 148.8, HCO^{3-}: 4.2, HPO_4^{2-}: 1.0, Buffer, Tris, pH: 7.4 [32]). Samples were taken from the supernatant at each time point (0, 1, 3, 7, 14, 30 days). The concentrations of Ca^{2+}, P^{5+}, Mg^{2+}, $Zn^{2+}$and Sr^{2+} ions in simulated SBF solutions were measured. Only the excess amount of calcium, magnesium, and phosphorous was taken into account for the evaluation of the dissolution of different ions.

3. Results and discussion

3.1. Morphological characteristics of cACP powder coating, PCL and cAPC-PCL composite layers

Thorough morphological characterization of the PCL layer as well as cACP particles and cACP-loaded PCL composites was carried out by SEM observation. As Fig. 1 demonstrates, the cACP particles are mainly globular shaped, and the sizes of individual particles vary between 100 and 500 nm. In addition, some larger, cubic, and elongated rectangle-shaped particles are also visible. This kind of shape of ACP particles is reported in many research works [33–37]. The bioactive ion doping, applied in low concentrations, did not cause any significant change in the morphology of cACP particles (Fig. 1).

As Fig. 1 (c) shows, all the doping elements are incorporated successfully into the cACP particles. The carbon signal might come from the carbonate content within the powder. There are significant signals of Ti and Al also, which indicates that the coating is very thin and non-continuous. The morphology of pure PCL and the cACP-PCL composite layers and the thickness of the layers were also investigated (Fig. 2).

The pure PCL layer, prepared by spin coating, presents several holes and an amorphous, non-continuous structure. The surface of the substrate is also discernible through the holes. The cACP-PCL composite layer, prepared in the same way, shows significantly different micro-

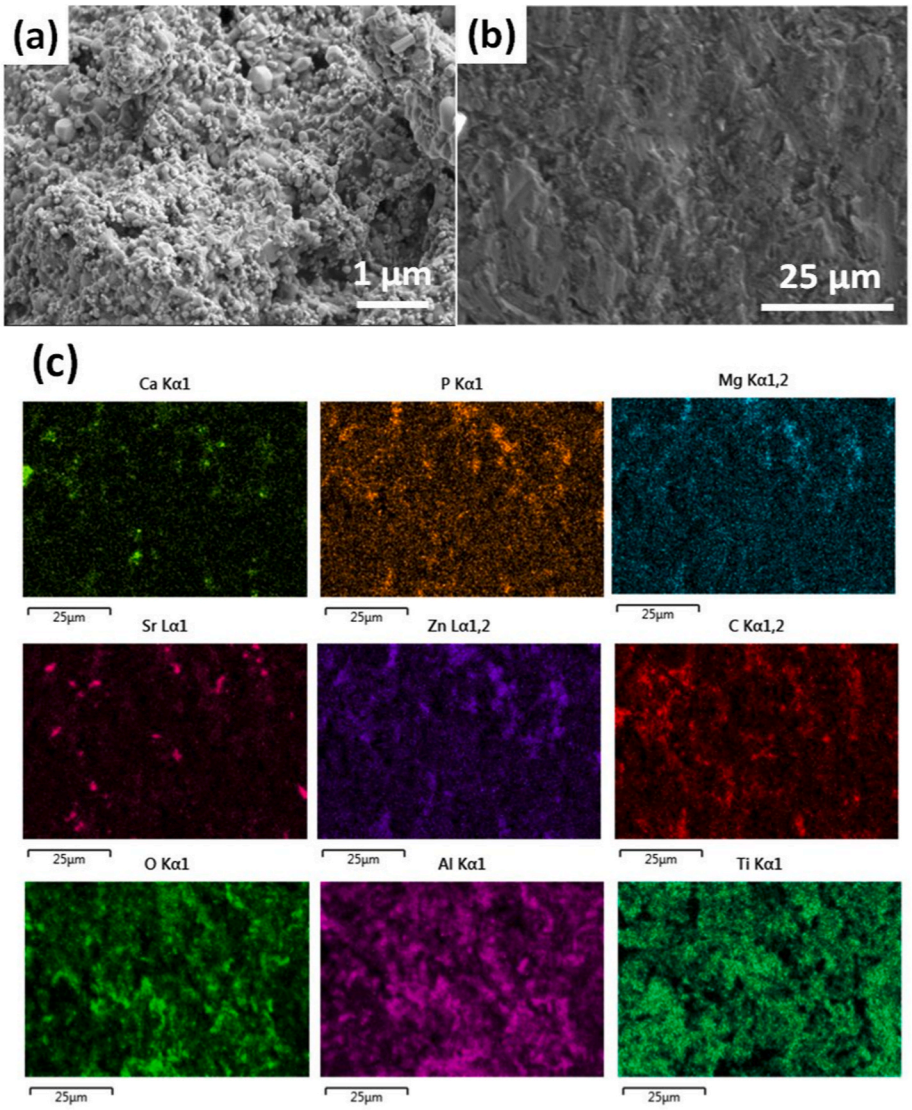

Fig. 1. SEM image 20kX (a) as well as the electron image (b) and the corresponding elemental mapping (c) of cACP particles.

and nanostructures. The SEM images (Fig. 2 b) clearly reveal that the smaller cACP particles are embedded into the larger polymer particles, which are present mainly in large plate forms. The small, spheroid cACP particles are in between the PCL plates, and are also deposited onto the surface of the PCL plates in spots. SEM-FIB measurements were performed on different sites of the cACP-coated sample as well as on the cACP-PCL composite layer to reveal their thickness. As Fig. 2 (c) and (d) display, the coatings are very thin, the thickness ranges between around 230 nm–1700 nm in the investigated areas, however, owing to the substrate's very rough surface there are also uncovered areas (see in Fig. 1 (c) elemental maps). It is clearly visible that the structure of the coatings is very porous with many holes inside. This structure is very similar to the natural bones which can make the implant more biocompatible allowing the adhesion and growth of bone cells. It is widely reported that porous structures are appropriately advantageous for bone cell adhesion and can promote cell growth [38,39]. The interconnected pore structure allows inwards diffusion of oxygen and nutrients and outwards diffusion of waste products, supporting cell migration into the coating and increasing the available surface area for cell adherence [40–44]. Even though being biocompatible is essential for an implant coating, an ideal bone substitute material should have a fully interconnected porous structure to allow for bone ingrowth, besides, it should degrade in the human body as the bone regenerates [45,46].

The elemental composition of cACP powder determined by the ICP-AES technique is presented in Table 1.

As can be seen in Table 1, the elemental composition of the precipitated powder is slightly different from the concentration of chemicals used in the wet chemical reaction. Mg and Zn are present in higher concentrations in the cACP, while the strontium content hardly changed. The reason for this behavior can be explained by the favorable apatite-forming ability of both magnesium and zinc. Since the atomic radii of Mg^{2+} and Zn^{2+} are 72 p.m. and 74 p.m., respectively, they are smaller than the Ca^{2+} ion (100 p.m.). This might allow them easier incorporation into the CaP phase than in the case of larger Sr ions (118 p.m.). The measured Ca:Mg:Zn:Sr weight ratio in the precipitated powder is 88.72:9.18:2:0.1. The calculated Ca/P ratio was around 2.05 which is close to the reported elemental ratio in human bones [47–49]. This Ca/P ratio was also measured in different ACP phases [13,50,51]. There are reports describing that Mg and Zn can incorporate into the CaP phases and form magnesium whitlockite ($Ca_{18}Mg_2(HPO_4)_2(PO_4)_{12}$) [52] as well as parascholzite ($CaZn_2(PO_4)_2{\cdot}2(H_2O)$) phases [53,54]. Strontium can also precipitate as different $Ca_{(3-x)}Sr_x(PO_4)_2$ phosphates or strontium apatite $(Sr,Ca)_5(PO_4)_3(OH,F)$ [55–59].

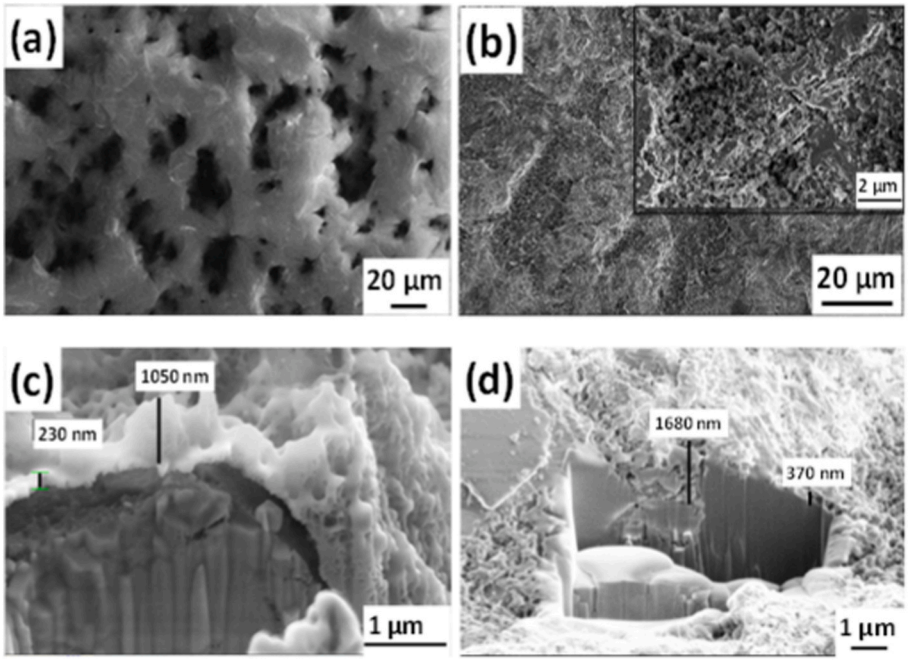

Fig. 2. SEM image of pure PCL layer 5kX (a) the cACP-PCL composite with a magnification of 1kX (b) and with a magnification of 10kX (inset) as well as SEM-FIB cross-sectional cut of cACP powder layer (c) and cACP-PCL composite layer (d).

Table 1
Mean (±SD) elemental percentages in Wt.% of the cACP powder (N = 3).

Element	Ca	P	Mg	Zn	Sr	Ca/P	(Ca + Mg + Zn + Sr)/P
Ratio in Wt.%	61.88 ± 3.50	30.24 ± 1.24	6.41 ± 0.92	1.40 ± 0.10	0.07 ± 0.01	2.05	2.31

3.2. Surface roughness measurements

The roughness of the surface is also a crucial factor for the adoption of implants by the human body. It is extensively reported that rougher surfaces are very advantageous for the attachment of bone cells [60,61]. Fig. 3 demonstrates the result of surface roughness measurements on the substrate and on different coatings investigated.

As the total roughness profile shows, the difference between the highest and deepest points in the surface was 6.96 µm for Ti6Al4V, 5.94 µm for the PCL coating, 12.16 µm for the cACP coating, and 7.51 µm for the cACP-PCL composite. Therefore, the measurements revealed that the cACP powder coating increased the roughness due to the uneven deposition and that the powder particles tended to agglomerate into

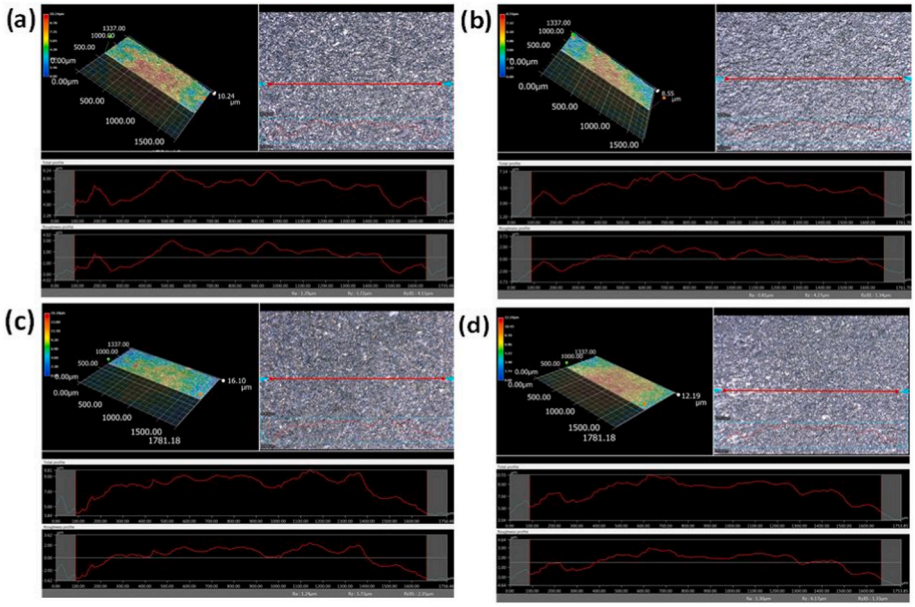

Fig. 3. Optical microscope images and surface roughness of Ti6Al4V substrate (a), PCL coating (b), cACP coating (c), as well as a cACP-PCL composite coating (d).

larger parts on different sites of the samples. The distribution of PCL coating was more homogeneous, which lead to a smoother surface. The cACP-PCL coating also caused a slight increase in surface roughness. It is discussed that the roughness and the hydrophilicity of the surface are directly correlated [62–64] while promoting the spreading and differentiation of osteoblasts [65–67].

The parameters of the surface roughness of different samples are shown in Table 2.

3.3. In vitro biocompatibility tests

3.3.1. Cell viability

Cell Counting Kit-8 (CCK-8) allows very convenient assays by utilizing the highly water-soluble tetrazolium salt WST-8 [2-(2-methoxy-4-nitrophenyl)-3-(4-nitrophenyl)-5-(2,4-disulfophenyl)-2H-tetrazolium, monosodium salt] produces a water-soluble formazan dye upon reduction in the presence of an electron carrier. In principle, WST-8 is reduced by dehydrogenases in cells to give a yellow-colored product (formazan), which is soluble in the tissue culture medium. The amount of the formazan dye generated by the activity of dehydrogenases in cells is directly proportional to the number of living cells.

The cell viability studies (Fig. 4 a and b) clearly revealed that both the cACP powder coatings and the cACP -PCL composite coatings improved the *in vitro* biocompatibility of implant material. The number of cells on samples increased exponentially over time. The highest values were measured in the case of the bioactive ions doped hydroxyapatite (cACP) with around 98% cell viability. However, the cell viability on all types of composite coatings was over 80% at all investigated culture times which proves their superior biocompatibility to uncoated substrates. The reason for the enhanced biocompatibility of both cACP and cACP-PCL composite coating might be that they can provide a better micro-environment for cell adherence and growth compared to the substrate or the pure PCL coating.

The statistical diagrams (Fig. 4 c-f) show the level of statistical significance between all investigated groups. If P values are less than 0.05, that means the difference in values of compared groups is statistically significant. The analysis revealed that after one day of cell culture, there are five out of ten statistically different groups, namely, the cACP-PCL/PCL, the cACP/PCL, the cACP/Ti6Al4V, PCL/positive control, and the Ti6Al4V/positive control. After three-day cell culture, the number of statistically different groups increased (7 out of 10). However, after one or two weeks of cell culture, an almost similar tendency can be observed.

3.3.2. Cell amount and enzyme activity

Lactate dehydrogenase (LDH) activity measures the number of attached cells on the samples while ALP values are also a relevant indicator of viable cells and are considered to detect the presence of osteoblast cells and the formation of new bone.

The LDH activity (Fig. 5 a) values showed that there were living cells on all samples. There were more living cells on the surface of ACP and cACP-PCL coated samples (both in powder and composite form) than in the case of uncoated titanium alloy after one and two weeks of immersion and culturing in DMEM medium. The highest number of cells was measured on cACP coating compared to positive control and the cACP powder addition to the pure PCL polymer increased slightly its biocompatibility. The ALP activity measurements (Fig. 5 b) (transformation rate of p-nitrophenyl phosphate into p-nitrophenol) showed a very similar tendency to that for ALP. Similarly, the highest LDH values were measured in the cases of cACP and cACP-PCL coatings. The statistical analysis of both LDH and ALP measurements showed a very similar tendency. The measured LDH and ALP values were statistically highly significant between the control group and the Ti alloy substrate (***$p < 0.001$) and the PCL coating (**$p < 0.01$) as well as the differences between the values of cACP-PCL thin layer and the Ti alloy were also statistically significant (*$p < 0.05$) at the 7th day of cell culture. On the other hand, at the 14th day of cell culture, the difference between the measured LDH and ALP values became less statistically significant, however, the tendency remained. This can indicate that the pre-osteoblast cells need more time to attach and grow on the surface of Ti alloy and pure PCL coating due to the less advantageous environment than in the case of ACP-containing coatings (cACP and cACP-PCL). In conclusion, both LDH and ALP activities were the lowest in the case of substrate material and the PCL coating. These results are in good accordance with other works, in which different calcium phosphate phases and CaP-polymer composites were investigated regarding their osteogenic activities [68–73]. Tas et al. [68] studied the osteoclast responses to the tricalcium phosphate (TCP) phases in zinc and to zinc-doped TCP-containing culture medium. They found that the zinc content led to an increase in osteoblast cell proliferation, ALP activities, and bone formation because of the release of zinc ions. Fernandes et al. [69] prepared hydroxyapatite nanoparticles, containing citrate and zinc ions (cit-Zn-Hap). In their experiments, increased ALP activity was measured for the cit-Zn-Hap samples. Schmidt et al. [70] studied the cell response to the electrochemically deposited Sr-substituted hydroxyapatite layers and reported increased ALP and LDH activities compared to the uncoated substrate. They observed that the Sr^{2+}-ions released from the coated samples stimulated the proliferation and differentiation of osteogenically induced hBMSC cells. In other research work [71], the osteogenic characteristics of strontium-silver co-substituted fluorohydroxyapatite (FHAp, SrAgFHAp, and AgHAp) were examined on osteoblast cells. They revealed that the ALP values of FHAp and SrAgFHAp coating were significantly higher than that of Ti and AgFHAp, while the ALP values of osteoblasts on AgHAp were significantly reduced compared to FHAp owing to the cytotoxicity effect of silver. On the other hand, the measured LDH activity in the different groups was similar, showing no significant difference. This could indicate that the SrAgFHA coating was also biocompatible, and the cytotoxicity of Ag ions was not significant in their case. The biocompatibility characteristics of multi-substituted (Mg, Sr, Si, F) calcium phosphate (Ca9·5Mg0·25Sr0·25(PO4)5·5(SiO4)0·5(OH)1·2F0.8) on MG63 osteoblast-like cells were also reported by Kheradmandfard et al. [72]. Similarly to the previously mentioned research works, they also concluded that the Si, Mg, Sr, and F in the SHAp samples promoted osteoblast differentiation and activity. In addition, the biocompatibility and osteogenic activity of calcium phosphate-biopolymer composites were also considered. He et al. [73] prepared electrospun polycaprolactone-hydroxyapatite-ZnO composite film (PCL-5%HA-1%ZnO) and studied the biocompatibility on MC3T3-E1 cells. Consistent with the other findings, they also measured increased ALP activity/osteogenesis for both PCL-5%HA and PCL-5% HA-1%ZnO layers and additionally the Zn content was more favorable.

Table 2
The variation of surface roughness parameters of investigated samples. Parameters are presented as arithmetic average roughness (Ra), the largest difference from peak-to-valley (Rz), and the Rz/Ra ratio[a]. The surface roughness was scanned at six different line profiles and the mean values ± SD are presented.

Samples	Ra/μm	Rz/μm	Rz/Ra
Ti6Al4V substrate	1.29 ± 0.34	5.72 ± 0.54	4.43
PCL layer	0.81 ± 0.13	4.47 ± 0.27	5.51
cACP layer	1.24 ± 0.22	5.73 ± 0.39	4.62
cACP-PCL layer	1.30 ± 0.19	6.17 ± 0.48	4.74

[a] The Rz/Ra ratio is an important parameter and is commonly used by both the industry and the research field to study the surface characteristics of materials.

3.3.3. Cell morphology

Calcein and DAPI staining were performed on cell-seeded samples to reveal the cell morphology. The samples were stained after 1 day of cell culture in DMEM medium.

As Fig. 6 shows, there are numerous living cells on all types of samples after one day of culture in DMEM medium. The density of cells appeared to be the less in the case of pure PCL coating which can be

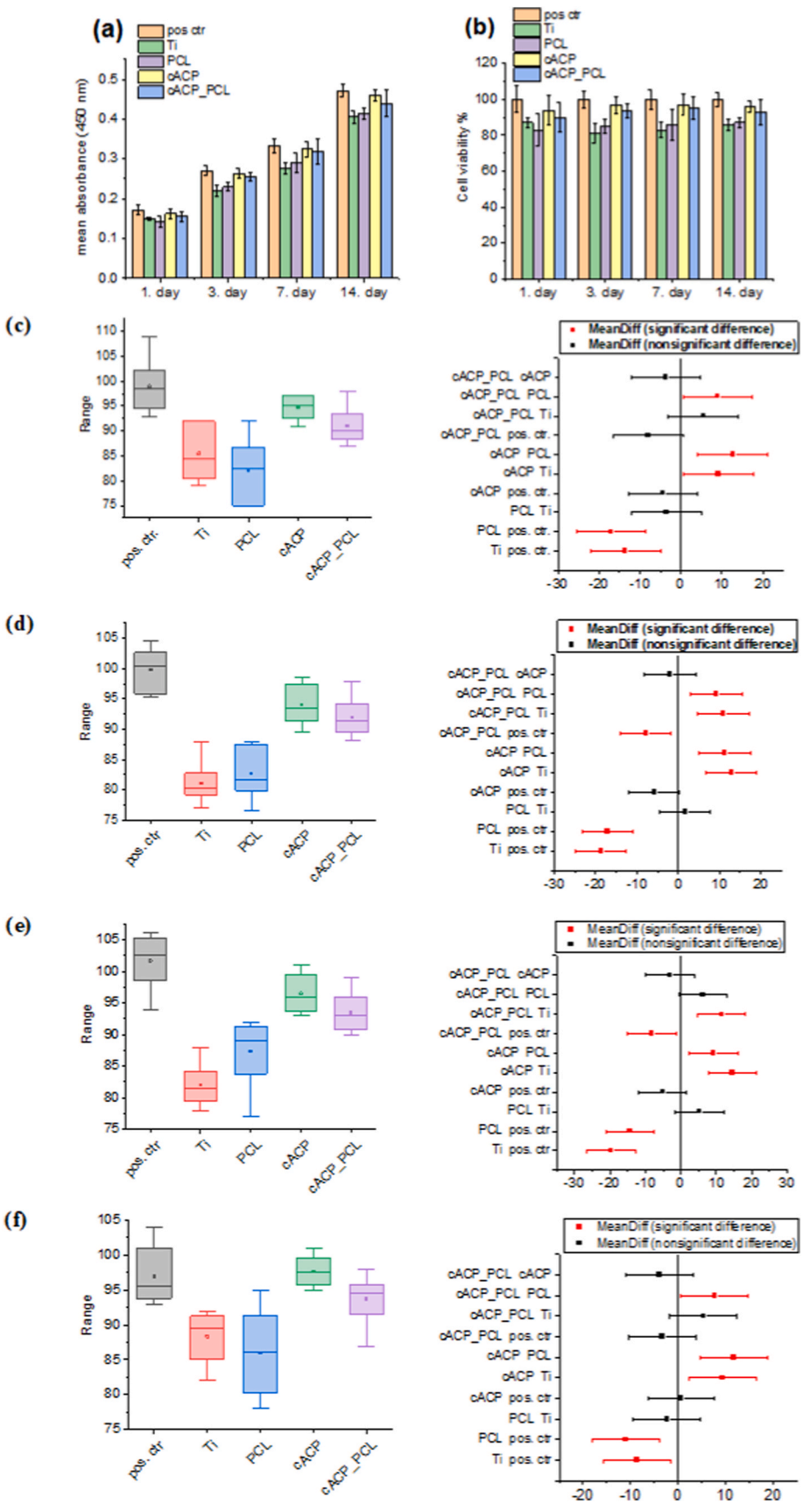

Fig. 4. Mean absorbance (±SD) of WST formazan generated by viable cells on uncoated and coated Ti6Al4V substrates (a) and normalized cell viability percentage compared to the positive control (b). Positive control (REF = 100%): MC3T3-E1 cells were grown in well plates without samples. Statistical analysis of the investigated samples after one day (c), three days (d) one week (e), and two weeks (f) of MC3T3-E1 cell culture. Significance level measured by P-value: if $P < 0.05$, the differences are statistically significant. Statistical analysis results on cell viability are shown in box charts representing the mean value ± standard deviation of six replicates of each sample type.

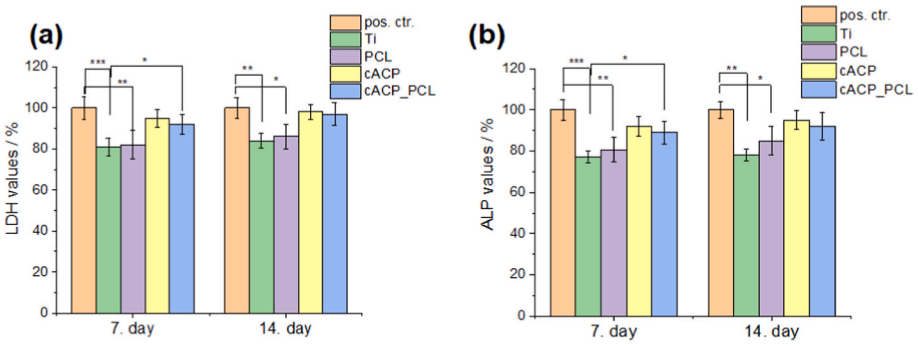

Fig. 5. LDH and ALP activity (mean percentages ± SD) on different samples. Positive control: MC3T3-E1 cells were grown in well plates without samples. All samples were measured in 6 replicates and calculated the mean values ± standard deviation (N = 6). Cells' death was induced by lysis buffer. The level of statistical significance was determined at *P* values: $*p < 0.05$ (significant), $**p < 0.01$ (highly significant), $***p < 0.001$ (more highly significant).

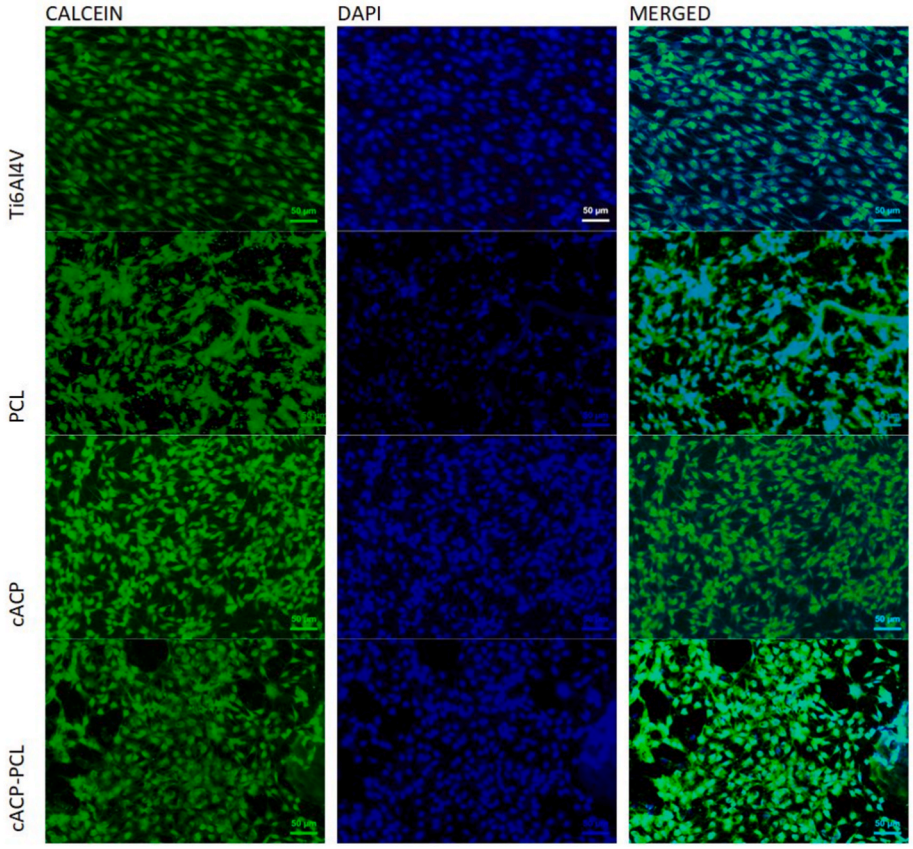

Fig. 6. Calcein, DAPI staining and their merged images on MC3T3-E1 cells seeded on investigated samples.

attributed to the fact that the hydrophilic PCL less advantageous to the cell's adhesion. On the other hand, very dense, homogeneous monolayers of cells are visible in the cases of Ti6Al4V substrate, the cACP coating, and also the cACP-PCL coating. The highest density was observed in the case of cACP powder coating, which is consistent with the results from the cell viability, ALP, and LDH measurements. It can be also observed that the cACP content in the PCL polymer significantly increased the biocompatibility since a denser and confluent cell layer was attached to the surface.

The morphology of adhered cells after 24 h of incubation in DMEM medium was further examined by SEM measurements (Fig. 7).

The pre-osteoblast cells exhibited normal morphology in all cases. A polygonal, wide-spreading shape is visible which is reported to be the ideal growth state of cells [74]. In addition, the cells have many protrusions such as filopodia and some flattened extensions, growing into the porous structure of layers. These cellular protrusions and extensions indicate well-adhered and migrating cells [63,75]. It is noteworthy that the cells on the cACP coating and the cACP-PCL coating are visibly well-spread with more protrusions than the cells on both the substrate material and the pure PCL coating. Moreover, according to the low-magnification SEM images, the cell density is the lowest for PCL coating, and the highest for cACP coating. In the cases of cACP and cACP-PCL coatings a very dense, coherent cell monolayer adhered to the surface. This is in good correlation with the result of cell staining experiments.

3.4. *In vitro study of bioactive ion dissolution*

The release of the bioactive ions during soaking in SBF solution at ambient temperature was followed over a long period of time (30 days)

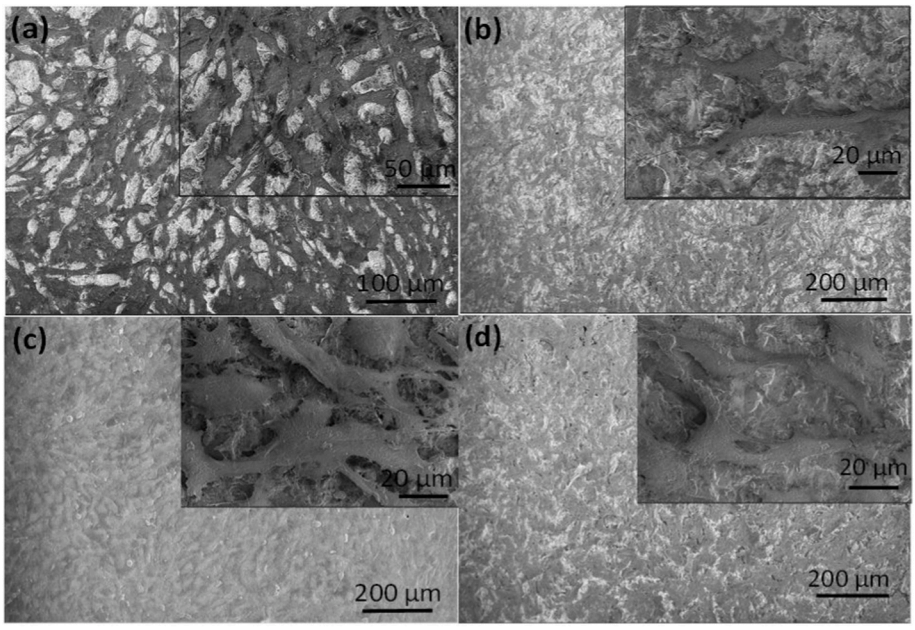

Fig. 7. SEM images of the MC3T3-E1 cell morphology after 24-h of incubation on Ti6Al4V samples: magnification 200X, in the inset 500× (a) on PCL layer: magnification 100X, in the inset 1000× (b) on cACP powder coating: magnification 100X, in the inset 1000× (c) and on cACP-PCL composite layer: magnification 100X, in the inset 1000X (d).

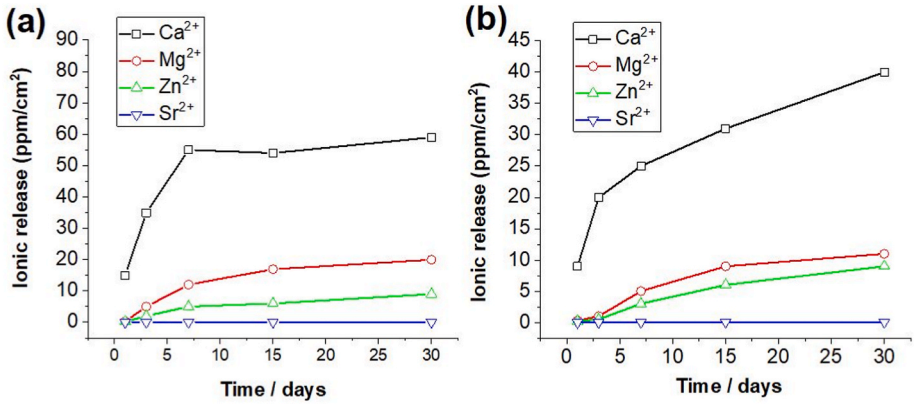

Fig. 8. Cumulative concentrations of the dissolved bioactive ions for cACP powder layer (a) and for cACP-PCL composite layer (b) soaked in SBF solution. The values are normalized to the unit area of samples. (Concentrations graphed as mean values ± SD, N = 3).

and is shown in Fig. 8.

It is visible that the concentrations of released bioactive ions are higher in the case of cACP sample which can be attributed to the larger number of particles per unit area. The profile of solubility is very similar for both samples (cACP and cACP-PCL). For cACP coating, the dissolution of Ca^{2+} ions follow a saturation curve, during the first week the dissolution rate is relatively fast, then it reaches a plateau with a stable and sustained release over time. This tendency is valid for the Mg^{2+} and Zn^{2+} ions also. On the other hand, the concentration of strontium hardly changes during the investigated period in both cases. For the cACP-PCL sample, the release profile of Ca^{2+} is slightly different, it shows an early-stage fast release, followed by continuous but significantly slower increasing tendency over time. This result can indicate that the biodegradability of the composite coating is faster than the one of the cACP powder layer. These results are in accordance with other reported works [37,76,77]. The calcium phosphate-containing PCL composites can be used and prepared in very various ways. For example, Lin et al. [78] studied the long-term *in vitro* degradation of polycaprolactone (PCL)/cobalt-substituted hydroxyapatite (CoHA) samples. They prepared the PCL composite as a membrane that contained 20 wt% CoHAp powders by solvent casting method. The developed membranes were immersed in phosphate buffer solution (PBS) for 6 months to follow their biodegradability. The experimental results revealed that adding HAp and CoHAp powders into the PCL matrix accelerated their biodegradation rate and changed the membrane's structure. On the other hand, the CaP-PCL composites can also be used as scaffold materials in bone tissue engineering. In a very recent work, Liu et al. [79] developed a scaffold material of PCL/TCP/PEG composite by 3D printing. They investigated the Ca and P ion release mechanism of the samples with different compositions by immersing them in an SBF solution over a long period. Similarly to our results, the ion release from the scaffolds demonstrated also a saturated curve feature. In other current research work [80] the dicalcium phosphate dihydrate (DCPD)/polycaprolactone composite was used as a corrosion-resistant coating on magnesium alloy substrates. The coating was prepared by a combination of electrodeposition and spin coating attaining a double layer in which the DCPD was the bottom layer and the PCL, incorporated with titania (TiO_2) was the sealing, outer layer. They also investigated the

degradation rate of the coating by electrochemical methods, recording potentiodynamic polarization curves. The results showed that owing to the sealing effect of the PCL layer and the blocking effect of TiO_2 nanoparticles, the composite coating significantly improved the corrosion resistance of the substrate, and the PCL layer hindered the dissolution of the calcium and phosphorous ions. Moreover, the TiO_2 addition further improved the biocompatibility of the substrate.

4. Conclusions

Biomimetic cACP powder was prepared by wet chemical precipitation and cACP as well as cACP-PCL composite layers were successfully deposited as very thin (230–1700 nm), non-continuous films onto commercially available, roughed titanium alloy substrate using spin coating. The morphological characterization showed the cACP particles to be dominantly in globular shape and the sizes of individual particles varied between 100 and 500 nm.

The bioactive ion doping in low concentrations did not cause any significant change in the morphology of cACP particles.

Cell viability measurements proved that the bioactive ions doped cACP coatings had the highest number of viable MC3T3-E1 cells compared to the uncoated substrate and the polymer coating after 1, 3, 7, and 14 days of culture. The cell viability on cACP and on the composite coatings was very high, around 98%, compared to the control group. The pure PCL coatings had almost similar biocompatibility properties to the titanium substrate, however, adding cACP powders into the polymer solution and applying them as a thin coating significantly increased the *in vitro* biocompatibility. Further measurements revealed many living cells on the surface of all samples. The cACP and the composite layer provided the highest number of living cells on their surface after one week and two weeks of culture. Fluorescence as well as the SEM images after one day of culture in DMEM also confirmed a large number of living and confluent, spread MC3T3-E1 cells with osteoblastic phenotype expression. The *in vitro* dissolution study indicated a slightly faster dissolution rate for the cACP-PCL composite coating than for the cACP powder coating. Overall, the present study confirms that bioactive ion-doped cACP-PCL coatings are favorable surface modifications for titanium alloy implants.

Declaration of competing interest

The authors declare that they have no known competing financial interests or personal relationships that could have appeared to influence the work reported in this paper.

Acknowledgment

The Authors are grateful for the SEM-FIB measurements to L. Illes and Z. Kovács, for the ICP-AES measurement to O. Czömpöly, for the biocompatibility tests to A. Grünewald. This work was supported by the National Research, Development and Innovation Office –NKFIH OTKA-PD 131934 and JECS TRUST (2021269) by the European Ceramic Society organization.

References

[1] N.S. Moghaddam, M.T. Andani, A. Amerinatanzi, C. Haberland, S. Huff, M. Miller, Mohammad Elahinia, David Dean, Metals for bone implants: safety, design, and efficacy, Biomanuf. Rev. 1 (1) (2016), https://doi.org/10.1007/s40898-016-0001-2.

[2] A.M. Keppler, M.M. Saller, P. Alberton, I. Westphal, F. Heidenau, V. Schönitzer, W. Böcker, C. Kammerlander, M. Schieker, A. Aszodi, C. Neuerburg, Bone defect reconstruction with a novel biomaterial containing calcium phosphate and aluminum oxide reinforcement, J. Orthop. Surg. Res. 15 (2020) 287–297, https://doi.org/10.1186/s13018-020-01801-8.

[3] J.C. Kim, M. Lee, I.-S.L. Yeo, Three interfaces of the dental implant system and their clinical effects on hard and soft tissues, Mater. Horiz. 9 (2022) 1387–1411, https://doi.org/10.1039/D1MH01621K.

[4] H.S. Alghamdi, Methods to improve osseointegration of dental implants in low quality (Type-IV) bone: an overview, J. Funct. Biomater. 9 (1) (2018) 7, https://doi.org/10.3390/jfb9010007.

[5] W. Habraken, P. Habibovic, M.E.M. Bohner, Calcium phosphates in biomedical applications: materials for the future? Mater. Today 19 (2) (2016) 69–87, https://doi.org/10.1016/j.mattod.2015.10.008.

[6] M. Canillas, P. Pena, A.H. de Aza, M.A. Rodríguez, Calcium phosphates for biomedical applications, Bol. Soc. Esp. Ceram. Vidr. 56 (2017) 91–112, https://doi.org/10.1016/j.bsecv.2017.05.001.

[7] X. Gao, M. Fraulob, Guillaume Haïat, Biomechanical behaviours of the bone–implant interface: a review, J. R. Soc. Interface 16 (156) (2019), 20190259, https://doi.org/10.1098/rsif.2019.0259.

[8] S. Parithimarkalaignan, T.V. Padmanabhan, Osseointegration: Update 13 (1) (2013) 2–6, https://doi.org/10.1007/s13191-013-0252-z.

[9] T. Wang, J. Bai, M. Lu, et al., Engineering immunomodulatory and osteoinductive implant surfaces via mussel adhesion-mediated ion coordination and molecular clicking, Nat. Commun. 13 (2022) AN160 1–A16017, https://doi.org/10.1038/s41467-021-27816-1.

[10] F. Barrére, C.A. van Blitterswijk, K. de Groot, Bone regeneration: molecular and cellular interactions with calcium phosphate ceramics, Int. J. Nanomed. 1 (3) (2006) 317–332. https://pubmed.ncbi.nlm.nih.gov/17717972/.

[11] L. Chen, J. Ren, N. Hu, Q. Du, D. Wei, Rapid structural regulation, apatite-inducing mechanism and *in vivo* investigation of microwave-assisted hydrothermally treated titania coating, RSC Adv. 11 (2021) 7305–7317, https://doi.org/10.1039/D0RA08511A.

[12] F. Zhang, A.J. Allen, L.E. Levine, M.D. Vaudin, D. Skrtic, J.M. Antonucci, K. M. Hoffman, A.A. Giuseppetti, J. Ilavsky, Structural and dynamical studies of acid-mediated conversion in amorphous-calcium-phosphate based dental composites, Dent. Mater. 30 (2014) 1113–1125, https://doi.org/10.1016/j.dental.2014.07.003.

[13] J. Zhao, Y. Liu, W. Sun, X. Yang, First detection, characterization, and application of amorphous calcium phosphate in dentistry, J. Dent. Sci. 7 (2012) 316–323, https://doi.org/10.1016/j.jds.2012.09.001.

[14] P. Osak, J. Maszybrocka, J. Kubisztal, P. Ratajczak, B. Łosiewicz, Long-term assessment of the *in vitro* corrosion resistance of biomimetic ACP coatings electrodeposited from an acetate bath, J. Funct. Biomater. 12 (2021) 1–16, https://doi.org/10.3390/jfb12010012, 12 doi.org/10.3390/jfb12010012.

[15] V.M. Wu, V. Uskoković, Is there a relationship between solubility and resorbability of different calcium phosphate phases in vitro? Biochim. Biophys. Acta 1860 (10) (2016) 2157–2168, https://doi.org/10.1016/j.bbagen.2016.05.022.

[16] L. Wang, G.H. Nancollas, Calcium orthophosphates: crystallization and dissolution, Chem. Rev. 108 (11) (2008) 4628–4669, https://doi.org/10.1021/cr0782574.

[17] J. Vecstaudza, M. Gasik, J. Locs, Amorphous calcium phosphate materials: formation, structure and thermal behaviour, J. Eur. Ceram. Soc. 39 (4) (2019) 1642–1649, https://doi.org/10.1016/j.jeurceramsoc.2018.11.003.

[18] L.D. Esposti, M. Iafisco, Amorphous calcium phosphate, the lack of order is an abundance of possibilities, Biomater. Biosystem 5 (2022), 100037, https://doi.org/10.1016/j.bbiosy.2021.100037.

[19] Y. Yang, G. Wang, G. Zhu, X. Xu, H. Pan, R. Tang, The effect of amorphous calcium phosphate on protein protection against thermal denaturation, Chem. Commun. 51 (41) (2015) 8705–8707, https://doi.org/10.1039/C5CC01420D.

[20] D.P. Minh, A. Nzihou, P. Sharrock, Carbonated hydroxyapatite starting from calcite and different orthophosphates under moderate hydrothermal conditions: synthesis and surface reactivity in simulated body fluid, Mater. Res. Bull. 60 (2014) 292–299, https://doi.org/10.1016/j.materresbull.2014.08.052.

[21] H. Madupalli, B. Pavan, M.M. J Tecklenburg, Carbonate substitution in the mineral component of bone: discriminating the structural changes, simultaneously imposed by carbonate in A and B sites of apatite, J. Solid State Chem. 255 (2017) 27–35, https://doi.org/10.1016/j.jssc.2017.07.025.

[22] R.S. Petersen, L.H. Nielsen, T. Rindzevicius, A. Boisen, S.S. Keller, Controlled drug release from biodegradable polymer matrix loaded in microcontainers using hot punching, Pharmaceutics 12 (2020) 1050, https://doi.org/10.3390/pharmaceutics12111050.

[23] G.C. Ebersole, E.G. Buettmann, M.R. MacEwan, M.E. Tang, M.M. Frisella, B. D. Matthews, C.R. Deeken, Development of novel electrospun absorbable polycaprolactone (PCL) scaffolds for hernia repair applications, Surg. Endosc. 26 (10) (2012) 2717–2728, https://doi.org/10.1007/s00464-012-2258-8.

[24] S. Wang, R. Gu, F. Wang, X. Zhao, F. Yang, Y. Xu, F. Yan, Y. Zhu, D. Xia, Y. Liu, 3D-Printed PCL/Zn scaffolds for bone regeneration with a dose-dependent effect on osteogenesis and osteoclastogenesis, Mater. Today Bio 13 (2022), 100202, https://doi.org/10.1016/j.mtbio.2021.100202.

[25] Y.K. Kim, K.B. Lee, S.Y. Kim, et al., Improvement of osteogenesis by a uniform PCL coating on a magnesium screw for biodegradable applications, Sci. Rep. 8 (2018), 13264, https://doi.org/10.1038/s41598-018-31359-9.

[26] C.X. Lam, D.W. Hutmacher, J.T. Schantz, H.S. Teoh, Evaluation of polycaprolactone scaffold degradation for 6 months *in vitro* and *in vivo*, J. Biomed. Mater. Res. 90 (3) (2009) 906–919, https://doi.org/10.1002/jbm.a.32052.

[27] B. Azimi, P. Nourpanah, M. Rabiee, S. Arbab, Poly (ϵ-caprolactone) fiber: an overview, J. Eng. Fibers Fabr. 9 (3) (2014) 74–90, https://doi.org/10.1177/155892501400900.

[28] P. A Gunatillake, A. Adhikari, Biodegradable synthetic polymers for tissue engineering, Eur. Cell. Mater. 20 (5) (2003) 1–16, https://doi.org/10.22203/ecm.v005a01.PMID:14562275.

[29] M.A. Woodruff, D.W. Hutmacher, The return of a forgotten polymer – polycaprolactone in the 21st century, Prog. Polym. Sci. 35 (2010) 1217–1256, https://doi.org/10.1016/j.progpolymsci.2010.04.002.

[30] W. Castro, J. Hoogewerff, C. Latkoczy, J.R. Almirall, Application of laser ablation (LA-ICP-SF-MS) for the elemental analysis of bone and teeth samples for discrimination purposes, Forensic Sci. Int. 195 (2010) 17–27, https://doi.org/10.1016/j.forsciint.2009.10.029.
[31] O.A. Golovanova, N.N. Strunina, S.A. Lemesheva, B.T. Baisova, Determination of the elemental composition of human bone tissue by atomic emission spectral analysis, J. Appl. Spectrosc. 78 (1) (2011) 157–160, https://doi.org/10.1007/s10812-011-9439-4.
[32] K. Tadashi, T. Hiroaki, How useful is SBF in predicting in vivo bone bioactivity? Biomaterials 27 (15) (2006) 2907–2915, https://doi.org/10.1016/j.biomaterials.2006.01.017.
[33] J. Vecstaudza, M. Gasik, J. Locs, Amorphous calcium phosphate materials: formation, structure and thermal behaviour, J. Eur. Ceram. Soc. 39 (2019) 1642–1649.
[34] M. Rivas, P. Turon, C. Alema, J. Puiggali, L.J. del Valle, Incorporation of functionalized calcium phosphate nanoparticles in living cells, J. Cluster Sci. 33 (2022) 2781–2795, https://doi.org/10.1007/s10876-021-02182-6.
[35] K. Rubenis, S. Zemjane, J. Vecstaudz, J. Bitenieks, J. Locs, Densification of amorphous calcium phosphate using principles of the cold sintering process, J. Eur. Ceram. Soc. 41 (2021) 912–919, https://doi.org/10.1016/j.jeurceramsoc.2020.08.074.
[36] T. Yu, J. Ye, M. Zhang, Effect of magnesium doping on hydration morphology and mechanical property of calcium phosphate cement under non-calcined synthesis condition, J. Am. Ceram. Soc. 96 (6) (2012) 1944–1950, https://doi.org/10.1111/jace.12235.
[37] J. Wu, K. Ueda, T. Narushima, Fabrication of Ag and Ta co-doped amorphous calcium phosphate coating films by radiofrequency magnetron sputtering and their antibacterial activity, Mater. Sci. Eng. C 109 (2020), 110599, https://doi.org/10.1016/j.msec.2019.110599.
[38] S. Fagerlund, J. Massera, N. Moritz, L. Hupa, M. Hupa, Phase composition and *in vitro* bioactivity of porous implants made of bioactive glass S53P4, Acta Biomater. 8 (2012) 2331–2339, https://doi.org/10.1016/j.actbio.2012.03.011.
[39] O. Gokcekaya, T.J. Webster, K. Ueda, T. Narushima, C. Ergun, *In vitro* performance of Ag-incorporated hydroxyapatite and its adhesive porous coatings deposited by electrostatic spraying, Mater. Sci. Eng. C 77 (2017) 556–564, https://doi.org/10.1016/j.msec.2017.03.233.
[40] C. Zhang, Y.Y. Hu, F.Z. Cui, S.M. Zhang, D.K. Ruan, A study on a tissue-engineered bone using rhBMP-2 induced periosteal cells with a porous nano-hydroxyapatite/collagen/poly(L-lactic acid) scaffold, Biomed. Mater. 1 (2) (2006) 56–62, https://doi.org/10.1088/1748-6041/1/2/002.
[41] K.A. Hing, S.M. Best, K.E. Tanner, W. Bonfield, P.A. Revell, Mediation of bone ingrowth in porous hydroxyapatite bone graft substitutes, J. Biomed. Mater. Res. 68 (1) (2004) 187–200, https://doi.org/10.1002/jbm.a.10050.
[42] F. Barrere, T.A. Mahmood, K. DeGroot, C.A. van Blitterswijk, Advanced biomaterials for skeletal tissue regeneration: instructive and smart functions, Mater. Sci. Eng. R Rep. 59 (1) (2008) 38–71, https://doi.org/10.1016/j.mser.2007.12.001.
[43] G. Turnbull, J. Clarke, F. Picard, P. Riches, L. Jia, F. Han, B. Li, W. Shu, 3D bioactive composite scaffolds for bone tissue engineering, Bioact. Mater. 3 (2018) 278–314, https://doi.org/10.1016/j.bioactmat.2017.10.001.
[44] M. Chen, Y. Sun, Y. Hou, Z. Luo, M. Li, Y. Wei, M. Chen, L. Tan, K. Cai, Y. Hu, Constructions of ROS-responsive titanium-hydroxyapatite implant for mesenchymal stem cell recruitment in peri-implant space and bone formation in osteoporosis microenvironment, Bioact. Mater. 18 (2022) 56–71, https://doi.org/10.1016/j.bioactmat.2022.02.006.
[45] Y. Li, J. Zhou, P. Pavanram, M.A. Leeflang, L.I. Fockaert, B. Pouran, N. Tümer, K.-Schröder, J.M.C. Mol, H. Weinans, H. Jahr, A.A. Zadpoor, Additively manufactured biodegradable porous magnesium, Acta Biomater. 67 (2018) 378–392, https://doi.org/10.1016/j.actbio.2017.12.008.
[46] W. Wang, G. Jia, Q. Wang, H. Huang, X. Li, H. Zeng, W. Ding, F. Witte, C. Zhang, W. Jia, G. Yuan, The *in vitro* and *in vivo* biological effects and osteogenic activity of novel biodegradable porous Mg alloy scaffolds, Mater. Des. 189 (2020), 108514, https://doi.org/10.1016/j.matdes.2020.108514.
[47] H.L. Jang, K. Jin, J. Lee, Y. Kim, S.H. Nahm, K.S. Hong, K.T. Nam, Revisiting whitlockite, the second most abundant biomineral in bone: nanocrystal synthesis in physiologically relevant conditions and biocompatibility evaluation, ACS Nano 8 (1) (2014) 634–641, https://doi.org/10.1021/nn405246h.
[48] R. Lagier, C.-A. Baud, Magnesium whitlockite, a calcium phosphate crystal of special interest in pathology, Patol. Res. Pract. 199 (5) (2003) 329–335, https://doi.org/10.1078/0344-0338-00425.
[49] M. Tzaphlidou, V. Zaichick, Calcium, phosphorus, calcium-phosphorus ratio in rib bone of healthy humans, Biol. Trace Elem. Res. 93 (1–3) (2003) 63–74, https://doi.org/10.1385/BTER:93:1-3:63.
[50] A.L. Boskey, Amorphous calcium phosphate: the contention of bone, J. Dent. Res. 76 (8) (1997) 1433–1436, https://doi.org/10.1177/00220345970760080501.
[51] D. Skrtic, J.M. Antonucci, JM. Bioactive polymeric composites for tooth mineral regeneration: physicochemical and cellular aspects, J. Funct. Biomater. 2 (3) (2011) 271–307, https://doi.org/10.3390/jfb2030271.
[52] S. Batool, U. Liaqat, Z. Hussain, M. Sohail, Synthesis, characterization and process optimization of bone whitlockite, Nanomaterials 10 (2020) 1856, https://doi.org/10.3390/nano10091856, doi:10.3390/nano10091856.
[53] M.H. Prado da Silva, F.N. Moura, D. Navarro da Rocha, L.A. Gobbo, A.M. Costa, L. H.L. Louro, Zinc-modified hydroxyapatite coatings obtained from parascholzite alkali conversion, Surf. Coating. Technol. 249 (2014) 109–117, https://doi.org/10.1016/j.surfcoat.2014.03.052.
[54] I.Y. Ortiz, A.R. Santosn, A.M. Costa, E. Mavropoulos, M.N. Tanaka, M.H. Prado da Silva, S. de Souza Camargo Jr., *In vitro* assessment of zinc apatite coatings on titanium surfaces, Ceram. Int. 42 (2016) 15502–15510, https://doi.org/10.1016/j.ceramint.2016.06.203.
[55] Y.C. Fredholm, N. Karpukhina, D.S. Brauer, J.R. Jones, R.V. Law, R.G. Hill, Influence of strontium for calcium substitution in bioactive glasses on degradation, ion release and apatite formation, J. R. Soc. Interface 9 (70) (2012) 880–889, https://doi.org/10.1098/rsif.2011.0387, 7.
[56] Z. Geng, S. Sang, S. Wang, F. Meng, Z. Li, S. Zhu, Z. Cui, Y. Jing, C. Wang, J. Su, Optimizing the strontium content to achieve an ideal osseointegration through balancing apatite-forming ability and osteogenic activity, Biomater. Adv. 133 (2022), 112647, https://doi.org/10.1016/j.msec.2022.112647.
[57] H. Pan, X. Zhao, B.W. Darvell, W.W. Lu, Apatite-formation ability – predictor of "bioactivity, Acta Biomater. 6 (2010) 4181–4188, https://doi.org/10.1016/j.actbio.2010.05.013.
[58] Y. Chen, Q. Guo, L. Liao, M. He, T. Zhou, L. Mei, M. Runowski, B. Ma, Preparation, crystal structure and luminescence properties of a novel single-phase red emitting phosphor CaSr2(PO4)2:Sm 3+ ,Li+, RSC Adv. 9 (2019) 4834–4842, https://doi.org/10.1039/C9RA00264B.
[59] A.R. Chakhmourarian, E.P. Reguir, R.H. Mitchell, Strontium-apatite: new occurrences, and the extent of Sr-for-Ca substitution in apatite-group minerals, Can. Mineral. 40 (2002) 121–136, https://doi.org/10.2113/gscanmin.40.1.121.
[60] E.V. Alakpa, K.E.V. Burgess, P. Chung, M.O. Riehle, N. Gadegaard, M.J. Dalby, M. Cusack, Nacre topography produces higher crystallinity in bone than chemically induced osteogenesis, ACS Nano 11 (2017) 6717–6727, https://doi.org/10.1021/acsnano.7b01044.
[61] B. Yuan, H. Chen, R. Zhao, X. Deng, G. Chen, X. Yang, Z. Xiao, A. Aurora, et al., Construction of a magnesium hydroxide/graphene oxide/hydroxyapatite composite coating on Mg–Ca–Zn–Ag alloy to inhibit bacterial infection and promote bone regeneration, Bioact. Mater. 18 (2022) 354–367, https://doi.org/10.1016/j.bioactmat.2022.02.030.
[62] J. Caballé-Serrano, A. Munar-Frau, L. Delgado, R. Pérez, F. Hernández-Alfaro, Physicochemical characterization of barrier membranes for bone regeneration, J. Mech. Behav. Biomed. Mater. 97 (2019) 13–20, https://doi.org/10.1016/j.jmbbm.2019.04.053.
[63] P. Jiang, Y. Zhang, R. Hu, X. Wang, Y. Lai, G. Rui, C. Lin, Hydroxyapatite-modified micro/nanostructured titania surfaces with different crystalline phases for osteoblast regulation, Bioact. Mater. 6 (2021) 1118–1129, https://doi.org/10.1016/j.bioactmat.2020.10.006.
[64] J. Wei, T. Igarashi, N. Okumori, T. Igarashi, T. Maetani, B. Liu, et al., Influence of surface wettability on competitive protein adsorption and initial attachment of osteoblasts, Biomed. Mater. 4 (4) (2009), 045002, https://doi.org/10.1088/1748-6041/4/4/045002.
[65] N. Zhang, W. Wang, X. Zhang, K.C. Nune, Y. Zhao, N. Liu, R.D.K. Misra, K. Yang, L. Tan, J. Yan, The effect of different coatings on bone response and degradation behavior of porous magnesium-strontium devices in segmental defect regeneration, Bioact. Mater. 6 (2021) 1765–1776, https://doi.org/10.1016/j.bioactmat.2020.11.026.
[66] S. Zheng, Q. Liu, J. He, X. Wang, K. Ye, X. Wang, C. Yan, P. Liu, J. Ding, Critical adhesion areas of cells on micro-nanopatterns, Nano Res. 15 (2022) 1623–1635, https://doi.org/10.1007/s12274-021-3711-6.
[67] J. Du, G. Wang, D. Song, J. Jiang, H. Jiang, J. Gao, In-vitro degradation behavior and biocompatibility of superhydrophilic hydroxyapatite coating on Mg-2Zn-Mn-Ca-Ce alloy, J. Mater. Res. Technol. 17 (2022) 2742–2754, https://doi.org/10.1016/j.jmrt.2022.01.155.
[68] A.C. Tas, S.B. Bhaduri, S. Jalota, Preparation of Zn doped β-tricalcium phosphate (β-ca3(po4)2) bioceramics, Mater. Sci. Eng. C 27 (2007) 394–401, https://doi.org/10.1016/j.msec.2006.05.051.
[69] M.H. Fernandes, M.M. Alves, M. Cebotarenco, I.A.C. Ribeiro, L. Grenho, P. S. Gomes, M.J. Carmezim, C.F. Santos, Citrate zinc hydroxyapatite nanorods with enhanced cytocompatibility and osteogenesis for bone regeneration, Mater. Sci. Eng. C 115 (2020), 111147, https://doi.org/10.1016/j.msec.2020.111147.
[70] R. Schmidt, A. Gebert, M. Schumacher, V. Hoffmann, A. Voss, S. Pilz, M. Uhlemann, A. Lode, M. Gelinsky, Electrodeposition of Sr-substituted hydroxyapatite on low modulus betatype Ti-45Nb and effect on *in vitro* Sr release and cell response, Mater. Sci. Eng. C 108 (2020), 110425, https://doi.org/10.1016/j.msec.2019.110425.
[71] X. Zhang, B. Wang, L. Ma, L. Xie, H. Yang, Y. Li, S. Wang, H. Qiao, H. Lin, J. Lan, Y. Huang, Chemical stability, antibacterial and osteogenic activities study of strontium-silver co-substituted fluorohydroxyapatite nanopillars: a potential multifunctional biological coating, Ceram. Int. 46 (2020) 27758–27773, https://doi.org/10.1016/j.ceramint.2020.07.275.
[72] M. Kheradmandfard, K. Mahdavi, A.Z. Kharazi, S.F. Kashani-Bozorgc, D.-E. Kim, *In vitro* study of a novel multi-substituted hydroxyapatite nanopowder synthesized by an ultra-fast, efficient and green microwave-assisted method, Mater. Sci. Eng. C 117 (2020), 111310, https://doi.org/10.1016/j.msec.2020.111310.
[73] X. He, Z. Huang, W. Liu, Y. Liu, H. Qian, T. Lei, L. Hua, Y. Hu, Y. Zhang, P. Lei, Electrospun polycaprolactone/hydroxyapatite/ZnO films as potential biomaterials for application in bone-tendon interface repair, Colloids Surf. B Biointerfaces 204 (2021), 111825, https://doi.org/10.1016/j.colsurfb.2021.111825.
[74] Z. Chunyan, C. Lan, L. Jiajia, S. Dongwei, Z. Jun, L. Huinan, *In vitro* evaluation of degradation, cytocompatibility and antibacterial property of polycaprolactone/hydroxyapatite composite coating on bioresorbable magnesium alloy, J. Magn. Alloys 10 (8) (2022) 2252–2265, https://doi.org/10.1016/j.jma.2021.07.014.
[75] E.G. Long, M. Buluk, M.B. Gallagher, J.M. Schneider, J.L. Brown, Human mesenchymal stem cell morphology, migration, and differentiation on micro and

nano-textured titanium, Bioact. Mater. 4 (2019) 249–255, https://doi.org/10.1016/j.bioactmat.2019.08.001.

[76] J. Cao, R. Lian, X. Jiang, A.V. Rogachev, *In vitro* degradation assessment of calcium fluoride-doped hydroxyapatite coating prepared by pulsed laser deposition, Surf. Coating. Technol. 416 (2021), 127177, https://doi.org/10.1016/j.surfcoat.2021.127177.

[77] A.A. Amany, M.K. Ahmed, Fibrous scaffolds of Ag/Fe co-doped hydroxyapatite encapsulated into polycaprolactone: morphology, mechanical and *in vitro* cell adhesion, Int. J. Pharm. 601 (2021), 120557, https://doi.org/10.1016/j.ijpharm.2021.120557.

[78] W.-C. Lin, C. Yao, T.-Y. Huang, S.-J. Cheng, C.-M. Tang, Long-term in vitro degradation behavior and biocompatibility of polycaprolactone/cobalt-substituted hydroxyapatite composite for bone tissue engineering, Dent. Mater. 35 (2019) 751–762, https://doi.org/10.1016/j.dental.2019.02.023.

[79] K. Liu, J. Sun, Q. Zhu, X. Jin, Z. Zhang, Z. Zhao, G. Chen, C. Wang, H. Jiang, P. Zhang, Microstructures and properties of polycaprolactone/tricalcium phosphate scaffolds containing polyethylene glycol fabricated by 3D printing, Ceram. Int. 48 (2022) 24032–24043, https://doi.org/10.1016/j.ceramint.2022.05.081.

[80] Y. Xu, T. Wang, X. Qu, Z. Liu, Y. Guo, G. Li, Z. Zhang, J. Lian, L. Ren, Preparation of anticorrosion, biocompatible and antibacterial dicalcium phosphate dihydrate/polycaprolactone-titania composite coating on Mg alloy, Prog. Org. Coating 172 (2022), 107133, https://doi.org/10.1016/j.porgcoat.2022.107133.